Free-positioning wireless power transfer for multiple-receivers using a half-cube shaped transmitting coil

Ibtisam Naveed[1*], Linlin Tan[1*], Muhammad Zubair Yameen[2] and Adil Hussain[3]

[1] *School of Electrical Engineering, Southeast University, Nanjing 210096, China*
[2] *School of Electrical Engineering, Yanshan University, Qinhuangdao 066004, China*
[3] *Huaneng Shandong Ruyi (Pakistan) Energy Pvt. Ltd. Sahiwal, Punjab 57000, Pakistan*
* Corresponding authors, E-mail: engribtisam@yahoo.com; tanlinlin@seu.edu.cn

Abstract

In recent developments, free-positioning wireless power transfer (WPT) systems have become a practical solution for simultaneously powering multiple devices. This paper proposes a half-cube-shaped transmitting coil for free-positioning multiple-receiver WPT systems. The receiving devices are placed inside the transmitter and charged effectively in spatial freedom. A rectangular coil and a smaller circular coil are utilized as receiving coils to investigate the performance of the WPT system in a typical application scenario. Practical experiments are implemented to evaluate the PTE depending on the receiver's movement. The results provide valuable insights into optimizing the design for spatially dynamic charging applications. Furthermore, the system's scalability suggests its potential utility in diverse multi-device charging scenarios. The measurement results demonstrate that the WPT system is capable of delivering 76.74% PTE for a single receiver, and 96.14% overall PTE to multiple receivers. Finally, a multiple-receiver wireless charging system using an RF-DC rectifier is designed to determine system efficiency, which demonstrates approximately 64% overall efficiency for charging multiple receivers simultaneously.

Introduction

Wireless power transfer (WPT) offers a practical and efficient method for delivering energy to electronic devices across various applications, including electric vehicles, medical implants, and consumer electronics[1–7]. With the rapid increase of portable devices, there is a growing need to design wireless charging systems that can simultaneously power multiple devices[8–10]. To achieve this, multiple-receiver (Rx) WPT systems have been explored to address system issues, including impedance-matching networks, and cross-coupling effects[11–15]. However, receiving devices often vary in dimensions, positions, and orientations. Free-positioning WPT offers a promising solution for reliable wireless charging of multiple devices, regardless of their arrangement or position[11,16–20]. This advancement enables more flexible deployment in everyday applications, eliminating the need for precise receiver positioning. It enhances the practicality of wireless charging in environments where mobility and spatial freedom are essential.

One proposed approach involves a bowl-shaped transmitter (Tx) structure designed to wirelessly charge a hearing aid[16]. This design, however, presents limitations, as it generates a narrow dead-zone near the center of the Tx coil in perpendicular arrangements. Another free-positioning Tx design, a half-rectangular prism structure has been proposed for consumer applications. While it reduces dead-zone issues, it still leaves a dead-zone at planes angled at 45° between adjacent coils[17]. Alternatively, controllable impedance matching networks have been proposed to achieve optimal power transfer efficiency (PTE) by automatically adjusting lumped element values[21–24]. However, the complexity of the control system poses challenges for practical implementation.

Figure 1 illustrates a typical free-positioning WPT system scenario for multiple devices. The consumer devices are placed freely inside the charging box, which is embedded in a Tx coil. The various Rx coils are based on the actual device shapes and designed with the impedance matching networks (IMN), and the RF-DC converters.

In this paper, we present a free-positioning WPT system for multiple-receiver applications. A half-cube-shaped Tx (HCS-Tx) structure is proposed whose field distribution analysis reveals robust and strong magnetic fields in the charging area. Moreover, two distinct receiver (Rx) configurations are adapted to evaluate the system's spatial performance. The mutual inductance between the HCS transmitter (Tx) and a moving receiver is determined through a mathematical approach. Circuit theory is employed to analyze the wireless power transfer (WPT) system with multiple receivers, deriving a generalized power transfer efficiency (PTE) function. An LCC matching network aligns the impedance of arbitrary coils with the source and load impedances. Both the Tx and Rx coils operate at 6.78 MHz, a frequency selected from the Industrial, Scientific, and Medical (ISM) radio bands.

The proposed design overcomes the limitations seen in previous systems, and lays the groundwork for a flexible, efficient, and scalable WPT framework suitable for diverse real-world applications.

The system fabrication and experiment is implemented to verify the PTE of the single Rx, as well as the multiple-receiver WPT system. A multiple-receiver wireless charging system is implemented with a double voltage rectifier. The overall system efficiency is evaluated depending on the input RF power, which presents a good performance of the multiple-receiver wireless charging system.

Free-positioning multiple-receivers WPT system analysis

In a magnetic resonant coupling WPT system, the efficiency of power transfer between coils is assessed by mutual inductance and the impedance matching network (IMN). The mutual inductance has been evaluated by the coil configuration and arrangement, which is
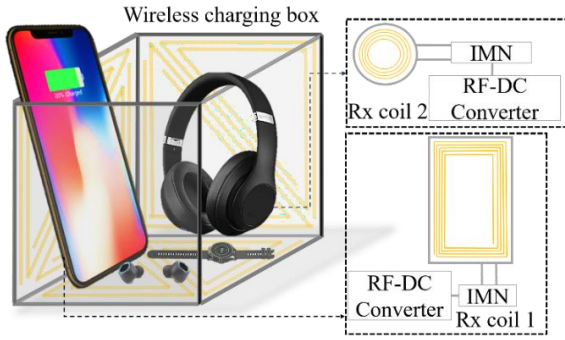
Fig. 1 Free-positioning for multiple-receivers WPT system.

significantly changed by varying the Rx position or rotating the Rx around its axis. Moreover, the coupling between two adjacent coils has also been decided by the magnetic flux with a stronger magnetic intensity, creating a higher mutual inductance. Therefore, the Rx coil will couple sufficiently with the Tx coil if it is placed in a strong magnetic field region. For a free-positioning WPT system, the Tx structure has been expected to generate a uniformly strong magnetic field to guarantee an effective power transfer on various positions of the Rx coil. To improve power delivery consistency, advanced coil arrangements, and field-shaping techniques can be utilized to maintain strong coupling across diverse Rx positions. Adaptive impedance matching further stabilizes system performance under varying load and alignment conditions. These strategies collectively support efficient and reliable multi-receiver operation in free-positioning WPT systems.

Free-positioning half-cube-shaped transmitter

To obtain a free-positioning power transfer, the produced magnetic field of the Tx coil has been required to achieve a strongly coupled magnetic field between Tx and Rx coils in the charging area. The HCS-Tx has been proposed with three orthogonal sub-coil planes, as shown in Fig. 2a. Each sub-coil plane consists of two triangular coil loops replacing the conventional rectangular coil to avoid the power-null point without using any additional compensation circuit[25–28]. In order to adapt the Rx rotation, the flowing current direction on each sub-coil plane is physically controlled as shown in Fig. 2a. Two consecutive sub-coils are connected by the connecting line on the bottom side of HCS-Tx. In addition, the current directions on two parallel coils have been arranged as identical to prevent the magnetic field elimination. The total magnetic field of the Tx coil has been increasingly contributed by the field elements generated from the sub-coils. Figure 2b–d illustrates the magnetic field distribution on three corresponding Cartesian coordinates of the HCS-Tx coil in Oxy, Oyz, and Ozx planes. The field pattern on each plane represents a strong magnetic field intensity that covers most of the Tx cross-sectional area. The printed spiral coil has been used to constitute the HCS-Tx structure due to its compact

characteristics. The magnetic field intensity is also decided by the number of turns, coil width, and the coil pitch respectively. For the proposed HCS-Tx coil structure, the five-turn triangular coil has been designed with a coil width w_{st} of 2.5 mm, and the coil pitch of 3.8 mm to obtain a strong magnetic field and low intrinsic resistance.

Calculation of mutual inductance

The mutual inductance between two wires is determined by evaluating Neumann's integral equation:

$$M_{12} = \left(\frac{\mu_0}{4\pi}\right) \oint_{L_t} \oint_{L_r} \frac{\vec{dl_t} \vec{dl_r}}{r} \tag{1}$$

where, L_t and L_r depict the Tx and Rx coil, $\vec{dl_t}$, and $\vec{dl_r}$ are the infinitesimal vectors, r is the distance between two vectors, and μ_0 is the permeability of free space.

The HCS-Tx structure is modeled to three square coil planes with each coil turn represented as a thin wire structure, as shown in Fig. 3. The coil plane dimensions are identical and determined by the coil length l_c. The ith coil turn is described by a vector $\vec{u_i}$, with its orientation defined by the direction of current flowing through that turn.

The Rx coil, on the other hand, is divided into straight segments, each of which is denoted by a vector $\vec{u_j}$. The overall mutual inductance is calculated by summing the individual mutual inductances between two coil vectors as expressed by Eq. (2).

$$M_{ij} = \frac{\mu_0}{4\pi} \sum_{i=1}^{C_i} \sum_{j=1}^{C_j} \frac{\vec{u_i} \cdot \vec{u_j}}{r_{ij}} \tag{2}$$

where, C_i denotes the number of vectors on Tx and C_j denote the number of vectors on Rx, and r_{ij} represents the distance between two vectors. The mutual inductance is investigated when moving Rx freely inside Tx to verify the stability of the mutual inductance value. The reference coordinate is illustrated by the coordinate variation of Rx center point. Specifically, the Cartesian movement is represented by $\vec{S}$ (d_x, d_y, d_z), while the angles φ_x, φ_y, and φ_z present the Rx rotation. The initialization position of Rx is given by $d_x = d_y = d_z = 0$ cm, and $\varphi_{xr} = \varphi_{yr} = \varphi_{zr} = 0°$, when the longest dimension of Rx is placed along Ox axis and its center point coincides with the origin point. Assume that the vector $\vec{u_j}$ at an arbitrary position of Rx is substituted by $\vec{u_j'}\left(x_j', y_j', z_j'\right)$, the mutual inductance between Rx and the HCS-Tx coil planes is given by the Eqs (3)–(5):

$$M_{P_1|Rx} = \frac{\mu_0}{4\pi} \sum_{j=1}^{C_j} \times$$

$$\left[\frac{2l_c z_j'}{\sqrt{x_j'^2 + y_j'^2 + \left(l_c - z_j'\right)^2}} - \frac{2l_c x_j'}{\sqrt{\left(l_c - x_j'\right)^2 + y_j'^2 + z_j'^2}} + \frac{l_c x_j' - l_c z_j'}{\sqrt{\left(l_c - x_j'\right)^2 + y_j'^2 + \left(l_c - z_j'\right)^2}} \right] \tag{3}$$
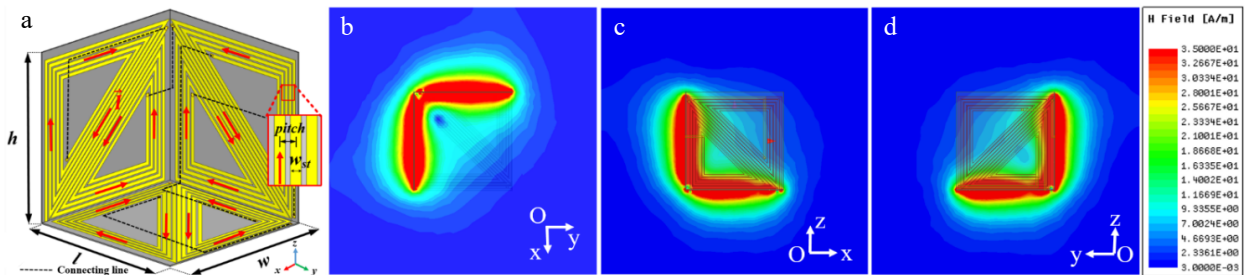

Fig. 2 (a) Proposed HCS-Tx coil: $l = 116$ mm, $w = 116$ mm, and $h = 116$ mm. (b)–(d) Magnetic field distribution on *Oxy*, *Oxz*, and *Oyz* planes.
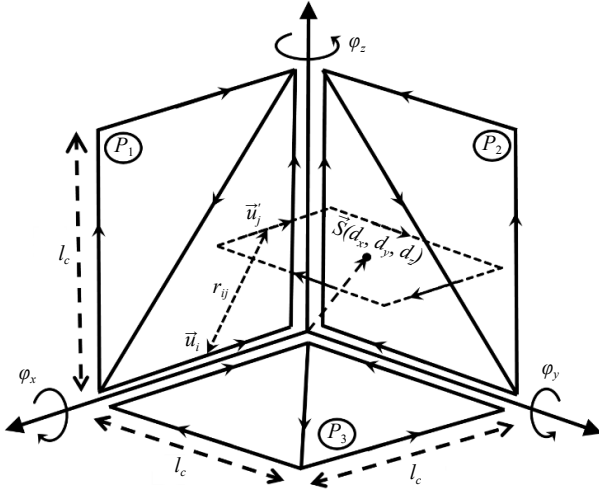
Fig. 3 Schematic illustration of the free-positioning WPT system.

Table 1. Extracted lumped element values.

FP HCS Tx		Rectangular Rx		Circular Rx	
Parameter	Value	Parameter	Value	Parameter	Value
L_{1t}	25.56 µH	L_{11}	6 µH	L_{12}	1.07 µH
R_{1t}	36 Ω	R_{11}	2.36 Ω	R_{12}	0.67 Ω
L_{pt}	8.2 µH	C_{11}	100 pF	C_{12}	655 pF
C_{1t}	85 pF	C_{21}	1 nF	C_{22}	2.4 nF
C_{2t}	1 pF	R_{L1}	50 Ω	R_{L2}	50 Ω
R_S	50 Ω				

$$M_{P_2|Rx} = \frac{\mu_0}{4\pi} \sum_{j=1}^{C_j} \times$$

$$\left[\frac{2l_c z_j'}{\sqrt{x_j'^2 + y_j'^2 + (l_c - z_j')^2}} - \frac{2l_c y_j'}{\sqrt{x_j'^2 + (l_c - y_j')^2 + z_j'^2}} + \frac{l_c y_j' - l_c z_j'}{\sqrt{x_j'^2 + (l_c - y_j')^2 + (l_c - z_j')^2}} \right] \quad (4)$$

$$M_{P_3|Rx} = \frac{\mu_0}{4\pi} \sum_{j=1}^{C_j} \times$$

$$\left[-\frac{2l_c x_j'}{\sqrt{(l_c - x_j')^2 + y_j'^2 + z_j'^2}} - \frac{2l_c y_j'}{\sqrt{x_j'^2 + (l_c - y_j')^2 + z_j'^2}} + \frac{l_c x_j' - l_c y_j'}{\sqrt{(l_c - x_j')^2 + (l_c - y_j')^2 + z_j'^2}} \right] \quad (5)$$

Table 1 presents key parameters, specific details, and essential components involved in the design and execution of circuits for the free-positioning wireless power transfer (WPT) system.

The total mutual inductance between the HCS-Tx and Rx coil can be computed by:

$$M_{12}^a = M_{P_1|Rx} + M_{P_2|Rx} + M_{P_3|Rx} \quad (6)$$

Power transfer efficiency formulation for multiple-receivers WPT system

Figure 4a shows the equivalent circuit and Fig. 4b represents the structural diagram of Multiple-receivers WPT. The equivalent Tx and Rx components are represented by their self-inductance L_{1x} and intrinsic resistances R_{1x} (x = t, 1, ..., n indicates the HCS-Tx coil and

each Rx coil). The mutual inductance between the HCS-Tx coil and each Rx coil is presented by M_{lx}. The cross-coupling between each Rx coil is neglected due to its small value compared to the mutual inductance. The source and load impedance R_X, R_{Li} are 50 Ω (i = 1, 2, ..., n indicates the Rx coils). Because of the longer physical length, the HCS-Tx coil presents a high characteristic impedance compared with the Rx coils. The LCC matching circuit is implemented on the HCS-Tx side and comprises a parallel inductor L_{pt} to reduce the input coil impedance. A series capacitor C_{1t} and a parallel capacitor C_{2t} are used to create resonant frequency and align the input coil impedance to source impedance. Meanwhile, on the Rx side, only a series capacitor C_{1i} and parallel capacitor C_{2i} (i = 1, 2, ..., n) are used due to the lower intrinsic resistance and inductance. The Tx coil impedance is given by:

$$Z_{Tx} = \left(\frac{1}{j\omega L_{1t}} + \frac{1}{R_{1t} + j\omega L_{1t}} \right)^{-1} \quad (7)$$

Thus, the total resistance and inductance on the Tx coil are given by:

$$R_{1t}' = \mathrm{Re}(Z_{Tx}) \quad (8)$$

$$Z_{L_{1t}}' = i \times \mathrm{Im}(Z_{Tx}) \quad (9)$$

The input impedance of the Tx and Rx coils are:

$$Z_t = R_{1t}' + Z_{L_{1t}}' \quad (10)$$

$$Z_i = R_{1i} + \frac{1}{j\omega C_{1i}} + j\omega L_{1i} \quad (11)$$

where, the component of Tx and the ith of Rx coil are indicated by t and i, respectively.

By using Kirchhoff's voltage law (KVL) on the Tx coil and reaching the Rx coil, the current relation between two arbitrary Rx coils is given by:
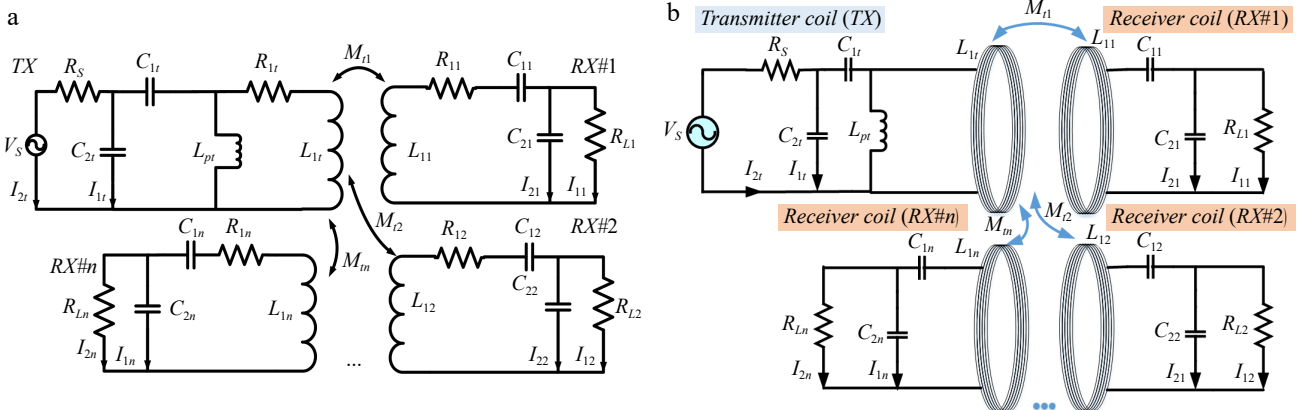

Fig. 4 (a) Multiple-receivers WPT equivalent circuit. (b) Structural diagram of Multiple-receivers WPT.

$$I_{2j} = I_{2i} \times \frac{\frac{Z_i}{Z_{M_{ti}}} \left(1 + \frac{Z_{C_{2i}}}{R_{L_i}} + \frac{Z_{C_{2i}}}{Z_i}\right)}{\frac{Z_j}{Z_{M_{tj}}} \left(1 + \frac{Z_{C_{2j}}}{R_{L_j}} + \frac{Z_{C_{2j}}}{Z_j}\right)} \quad (12)$$

The power transfer efficiency is also derived in Eq. (13), which is shown below. The resistance, capacitance, and inductance elements are given by:

$$\frac{V_S}{V_L} = -\frac{Z_{M_{ti}} R_S}{Z_{C_{2t}} Z_{C_{2i}}} \left(1 + \frac{Z_{C_{2i}}}{R_{Li}}\right)\left(1 + \frac{Z_{C_{2t}}}{R_S}\right)$$
$$+ \frac{R_S}{Z_{C_{2i}}} \left(\frac{Z_i}{Z_{M_{ti}}} + \frac{Z_i Z_{C_{2i}}}{Z_{M_{ti}} R_{Li}} + \frac{Z_{C_{2i}}}{Z_{M_{ti}}}\right)\left(\frac{Z_t^`}{Z_{C_{2i}}} + \frac{Z_t^` Z_{C_{2t}}}{R_S Z_{C_{2i}}} + 1\right)$$
$$- \frac{Z_i R_S}{Z_{M_{ti}} Z_{C_{2t}} Z_{C_{2i}}} \left(1 + \frac{Z_{C_{2i}}}{R_{Li}} + \frac{Z_{C_{2i}}}{Z_i}\right)\left(1 + \frac{Z_{C_{2t}}}{R_S}\right)$$
$$\times \sum_{j \neq i, j=i}^{n} \frac{1 + \frac{Z_{C_{2j}}}{R_{L_j}}}{\frac{Z_j}{Z_{M_{tj}}^2}\left(1 + \frac{Z_{C_{2j}}}{R_{L_j}} + \frac{Z_{C_{2j}}}{Z_j}\right)} \quad (13)$$

$$Z_{C_{1t}} = \frac{1}{j\omega C_{1t}}; \ Z_{L_{1t}} = j\omega L_{1t} \quad (14)$$

$$Z_{C_{1i}} = \frac{1}{j\omega C_{1i}}; \ Z_{C_{2i}} = \frac{1}{j\omega C_{2i}} \quad (15)$$

The equivalent scattering parameter S_{21} and the corresponding PTE are calculated using Eq. (17):

$$|S_{21}| = 2 \times \left|\frac{V_L}{V_S}\right| \times \sqrt{\frac{R_S}{R_L}} \quad (16)$$

$$PTE = |S_{21}|^2 \times 100\% \quad (17)$$

Experimental verification

The HCS-Tx and two Rx prototypes are constructed as illustrated in Fig. 5. The Taconic TLY substrate with the relative permittivity ε_r of 2.2, and a thickness of 0.8 mm is used due to its lightweight and low loss characteristics. A rectangular Rx is designed with a total dimension of 68 mm × 140 mm, and is supposed to be embedded in the smartphone device. Another circular Rx is designed for the smartwatch device with a diameter of 34 mm. The impedance matching circuits are integrated into the Tx and Rx on the same structures to reduce the system complexity. The extracted lumped elements of the Tx and Rx coils are listed in Table 1 including the coil characteristic impedance and values of matching elements.

Mutual inductance investigation

The mutual inductance is investigated for the HCS-Tx and rectangular Rx coil. The investigated results, as shown in Fig. 6 are
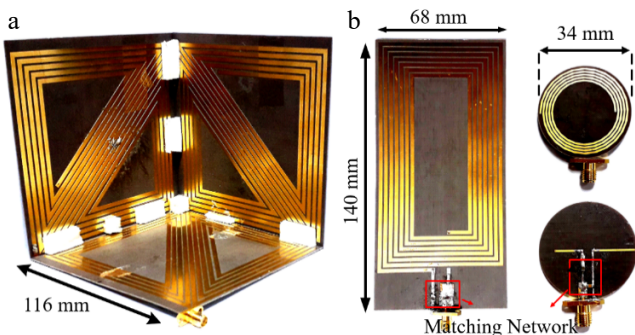
implemented for two cases. In the first case, the rectangular Rx is in line with the Oxz plane and moved along the Oy axis. Similarly, the second case is verified when the Rx coil is positioned orthogonal to the Oyz plane and moved along the Ox axis. The moving distances on the Ox and Oy axis of the Rx coil are indicated by p_x and p_y, respectively. The calculation results are solved by using the mutual inductance Eq (9). The simulation results are extracted from the ANSYS Electronics Desktop software, whereas the experimental results are acquired using the Protek A333 Vector Network Analyzer (VNA).

From the investigation results shown in Fig. 6, it is obvious that the mutual inductance presents stability with p_x and p_y varied from 10 to 80 mm on both of verification cases. This region corresponds to the active charging volume of the Tx coil due to the significant strong magnetic field distribution. The mutual inductance is highest when the Rx is placed at the center area around p_x and p_y of 50 mm with the values almost achieved higher than 800 nH. Moreover, as the Rx coil shifts farther from the central region, the mutual inductance drops significantly due to the increased separation between the Rx coil and the three Tx sub-coils. The results obtained through calculations, simulations, and measurements shows strong correlation. However, the measured values are slightly lower, which can be attributed to fabrication tolerances.

Single receiver WPT system

The coil-to-coil power transfer efficiency (PTE) is evaluated to demonstrate the free-positioning capability of the HCS-Tx structure using various placements of the rectangular Rx coil. These Rx positions are illustrated in the schematic diagram in Fig. 3. The movement of the rectangular Rx coil is defined by the displacement vector $\vec{S_r}(d_{xr}, d_{yr}, d_{zr})$ and the rotation angles $\varphi_{xr}, \varphi_{yr}, \varphi_{zr}$. Initially, the Rx coil is positioned at the coordinate origin with zero rotation angles. The experimental setup for the single rectangular receiver WPT system is depicted in Fig. 7a. Scattering parameters are measured using a two-port Vector Network Analyzer (VNA), Protek A333, with the HCS-Tx and Rx coils connected to Port 1 and Port 2, respectively. The coil-to-coil PTE is calculated according to the S_{21} parameter from Eq. (17).

The highest coil-to-coil PTE achieved in the experiment with the rectangular Rx coil is demonstrated in Fig. 7b, which corresponds to the movement vector and rotation angles of the Rx coil are $d_{xr} = 82$ mm, $d_{yr} = 26$ mm, $d_{zr} = 60$ mm, and $\varphi_{xr} = 65°, \varphi_{yr} = 0°, \varphi_{zr} = 0°$,

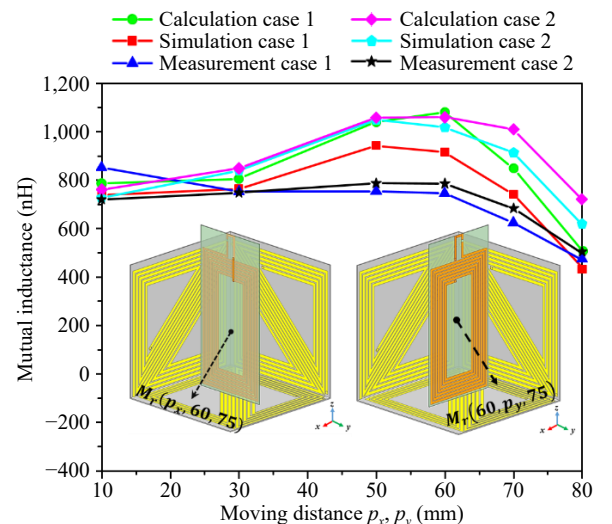**Fig. 5** (a) Fabricated HCS-Tx coil, (b) rectangular Rx coil, and (c) circular Rx coil.

Fig. 6 Mutual inductance between the HCS-Tx coil and rectangular Rx coil.
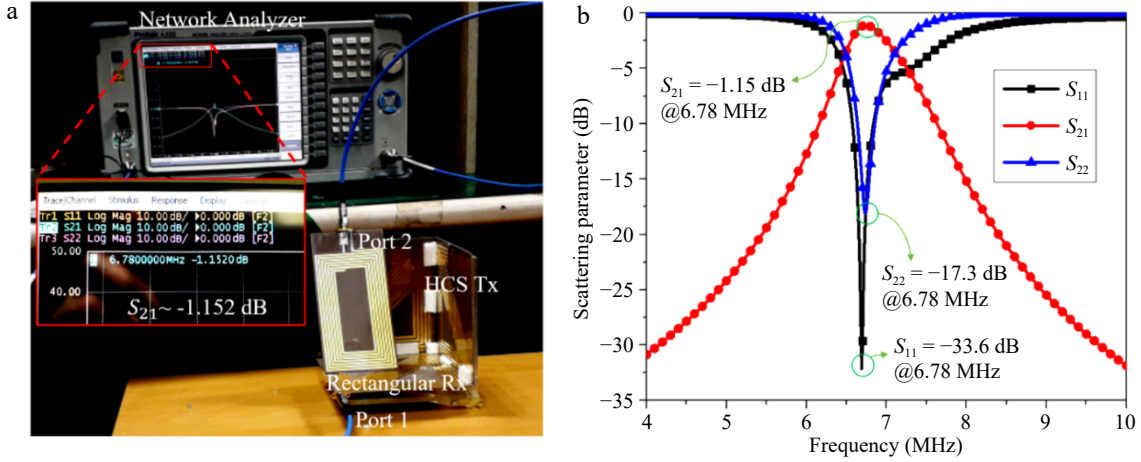
Fig. 7 (a) Single receiver WPT system measurement. (b) S-parameter results.

respectively. It is important to note that the reflection coefficients of both the Tx and Rx coils are minimal, owing to the effective impedance matching network designed for the operating frequency of 6.78 MHz. From Fig. 7b, the maximum transmission coefficient S_{21} achieves -1.15 dB at 6.78 MHz corresponding to the PTE of 76.74%. To validate the free-positioning WPT efficiency, the Rx coil is moved freely inside HCS-Tx structure. The coil-to-coil PTE is verified with the angular misalignment by varying the angles φ_{xr}, φ_{yr}, and φ_{zr}, respectively. Meanwhile, the axial misalignment is also considered by increasing the distance between rectangular Rx and the opposite HCS-Tx plane. To further ensure the robustness of the system, measurements were conducted under various misalignment scenarios, simulating real-world conditions where perfect alignment is rarely guaranteed. The system maintained consistent PTE across a broad range of orientations and distances, demonstrating the effectiveness of the HCS-Tx design. These results affirm the suitability of the proposed setup for practical, flexible charging environments. Figure 8 illustrates the coil-to-coil transmission efficiency as a function of the Rx coil's angular and axial misalignments.

The PTEs of rectangular Rx achieve a value of higher than 20% at almost all Rx arrangement scenarios, which shows the acceptable performance for a free-positioning WPT system. On the range of arrangement distance from 10 to 30 mm, the PTEs show an insignificant change as the Rx coil is rotated around its axis. Specifically, when the rotation angles φ_{zr} and φ_{xr} are varied with the step of 90°, the Rx coil is powered nearly uniformly because of the symmetrical Tx structure. In other words, by rotating Rx 45° around its axis, the PTEs present notable gaps because of the change in the direction of magnetic flux density. The Rx coil receives power the most effectively in the range from 10 to 60 mm, which corresponds to the strong magnetic field region. However, on the axial misalignment range from 60 to 80 mm, the PTEs present significant fluctuations at the axial misalignment positions because of the reduction in magnetic field intensity.

Multiple-receiver WPT system

To verify the performance of the free-positioning WPT system for multiple devices, the rectangular and circular Rx coils are placed inside the HCS-Tx coil simultaneously. The experiment is performed with some scenario arrangements of two Rx coils. The S-parameters of each Rx coil are measured alternately while another Rx coil is connected to the load of 50 Ω. The experiment provides the individual PTE of each Rx coil, and the overall PTE of the multiple-receivers WPT system is calculated by the sum of two individual PTEs. The positions of rectangular and circular Rx are illustrated respectively by the movement vector coordinates d_x, d_y, and d_z, and rotation angles φ_x, φ_y, and φ_z. The measured PTE results of the multiple-receivers WPT system are shown in Table. III with the highest overall PTE of 96.14%. The overall PTEs are stable on almost all positions of the two Rx coils, which are maintained at approximately 90% for measurement cases.

It is worth noting that the circular Rx achieves the more stable power transfer efficiency due to its smaller size compared with rectangular Rx. Specifically, the individual PTE of circular Rx remains at more than 20% for all of the verification scenarios, while the individual PTE of rectangular Rx has a significant gap between the highest and the lowest PTE approximating 15%.

Multiple-receivers wireless charging system

The performance of a free-positioning wireless charging system is validated with an arbitrary arrangement of the multiple-receivers system. The Rx circuit consists of an Rx coil, rectifier circuit, and a red LED to indicate charging status, as shown in Fig. 9a. A voltage doubler rectifier is used to convert the received RF power to an output DC voltage with high efficiency and output voltage. The use of two HSMS 2800 Schottky's diodes can enhance the input power range due to the breakdown voltage increase. The threshold voltage of the diode is V. The overall system efficiency is given by:

$$\eta_{sys} = \frac{V_{DC1}^2 + V_{DC2}^2}{R_{Load} \times P_{RF_{in}}} \times 100\% \tag{18}$$

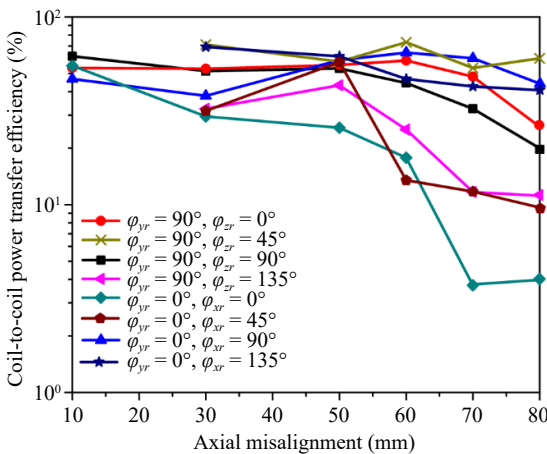where, $P_{RF_{in}}$ (W) indicates the input power supply, V_{DC1}(V) and V_{DC2}(V)
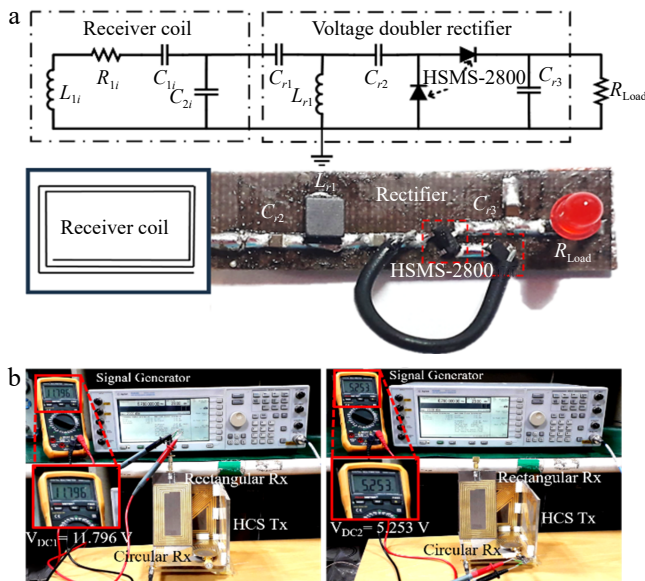

Fig. 8 Coil-to-coil power transfer efficiency.

Fig. 9 (a) Schematic diagram of Rx circuit: C_{r1} = 150 pF, L_{r1} = 3.3 μH, C_{r2} = 130 pF, C_{r3} = 1 F, R_{Load} = 1.3 kΩ. (b) Experimental setup for the multiple-receivers wireless charging system with the positions of Rx coil represented by d_{xr} = 82 mm, d_{yr} = 14 mm, d_{zr} = 65 mm, $\varphi_{xr} = \varphi_{yr} = \varphi_{zr}$ = 0°, d_{xc} = 80 mm, d_{yc} = 40 mm, d_{zc} = 5 mm, $\varphi_{xc} = \varphi_{yc} = \varphi_{zc}$ = 0°.

are the output DC voltages of the rectangular and circular Rx circuit, respectively.

The experimental validation of the proposed system is conducted by measuring the output voltage across each receiver (Rx) circuit under practical conditions. The half-cube-shaped transmitting coil (HCS-Tx) is powered by a signal generator (Agilent E4438C), delivering an input power level of 23 dBm. As a result of the wireless energy transfer, the output of the rectifying circuits connected to the rectangular and circular Rx coils achieves direct current (DC) voltages of approximately 11.8 and 5.2 V, respectively, as illustrated in Fig. 9b. These voltage levels reflect the capability of the system to maintain effective power delivery to multiple receivers, even when they differ in shape and position. By applying Eq. (18), which takes into account the input power and output DC levels, the overall

wireless charging system demonstrates an efficiency of approximately 64%.

To further illustrate the effectiveness of the proposed approach, Table 2 presents a performance comparison between this work and several recent studies in the field. The comparison includes critical parameters such as the wireless power transfer method, resonant operating frequency, physical dimensions of the transmitter coil, and the maximum achieved power transfer efficiency (PTE).

This analysis highlights the advantages of the HCS-Tx design in delivering high PTE and robust free-positioning capabilities, making it a strong candidate for real-world applications involving multiple, spatially flexible receivers.

The experiment results are obtained by measuring the output voltage on each Rx circuit. The HCS-Tx is supplied power of 23 dBm using the signal generator Agilent E4438C. The output rectified voltage of the rectangular and circular Rx circuit is approximately 11.8 and 5.2 VDC, respectively, as shown in Fig. 9b. By applying Eq. (18), the overall system efficiency is approximately 64%.

Table 3 presents an extensive comparison of wireless power transfer (WPT) systems operating at 6.78 MHz with multiple receivers, emphasizing power transfer efficiency. The data indicate that our proposed free-positioning WPT system, featuring the HCS-Tx structure, achieves an outstanding multi-receiver efficiency of 96.14%, surpassing all referenced works in this respect. Nevertheless, while this result is promising, further enhancements in overall system efficiency is needed to optimize power transfer performance even more.

Figure 10 visually illustrates the efficiency metrics of each WPT method, clearly showing the advantages of the half-cube-shaped transmitter (HCS-Tx) implemented in this study. Not only does the proposed system outperform existing designs in terms of multiple receiver efficiency, but it also demonstrates a competitive system-level efficiency of 64%. This graphical comparison underscores the robustness and effectiveness of the proposed free-positioning solution in practical multi-device charging scenarios.

Figure 11 offers a detailed overview of the performance and operational behavior of a wireless power transfer (WPT) system designed for a transmitter and multiple receivers. The first graph demonstrates the dynamic nature of the transmitter, showcasing periodic fluctuations in input voltage and current, with voltage oscillating

Table 2. Summary of measured power transfer efficiency of multiple-receivers WPT system.

Rectangular Rx							Circular Rx							Overall PTE
Coordinate (mm)			Angle (°)			PTE	Coordinate (mm)			Angle (°)			PTE	
d_{xr}	d_{yr}	d_{zr}	φ_{xr}	φ_{yr}	φ_{zr}		d_{xc}	d_{yc}	d_{zr}	φ_{xc}	φ_{yc}	φ_{zc}		
82	26	60	65	0	0	74.13%	35	85	5	0	0	0	20.42%	94.55%
82	26	60	65	0	0	73.79%	5	35	35	0	90	0	22.35%	96.14%
82	26	60	65	0	0	74.64%	5	80	80	0	90	0	20.42%	95.06%
82	14	65	70	0	0	65.77%	80	40	5	0	0	0	20.42%	86.19%
82	14	65	70	0	0	70.79%	80	40	5	0	0	0	22.38%	93.18%

Table 3. Performance Comparison of wireless power transfer (WPT) systems operating at 6.78 MHz with multiple receivers.

| WPT method	Resonant frequency (MHz)	Coil-to-coil transmission efficiency		System efficiency	Ref.
		Single Rx	Multiple Rx		
Planar Tx coil with switchable IMNs	6.78	82.1%	93%	NG	[11]
Class E amplifier with multiple receivers	6.78	NG	71.7%	NG	[29]
WPT system for multiple receivers operating at Inductive and Resonant Operating Modes	6.78	NG	83%	66%	[30]
WPT system for a dual-mode transmitter, along with two receivers	6.78	NG	78%	NG	[31]
Printed spiral half-cube shaped Tx structure	6.78	76.74%	96.14%	64%	This work
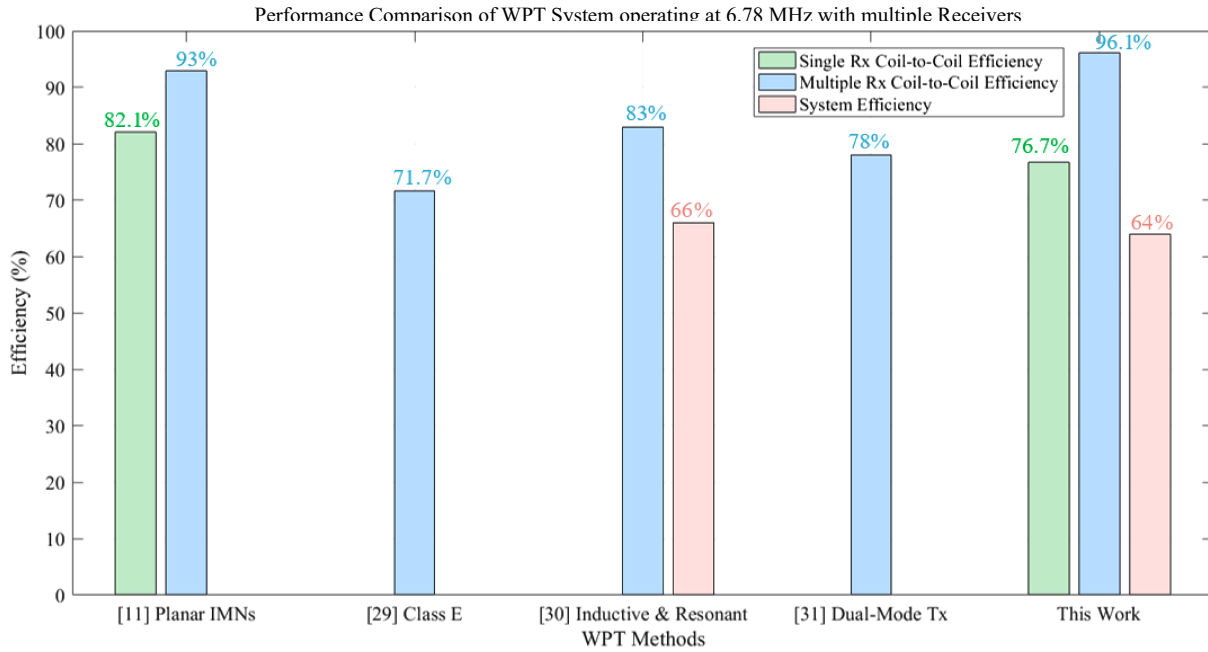
Fig. 10 Performance comparison of wireless power transfer (WPT) systems operating at 6.78 MHz with multiple receivers.
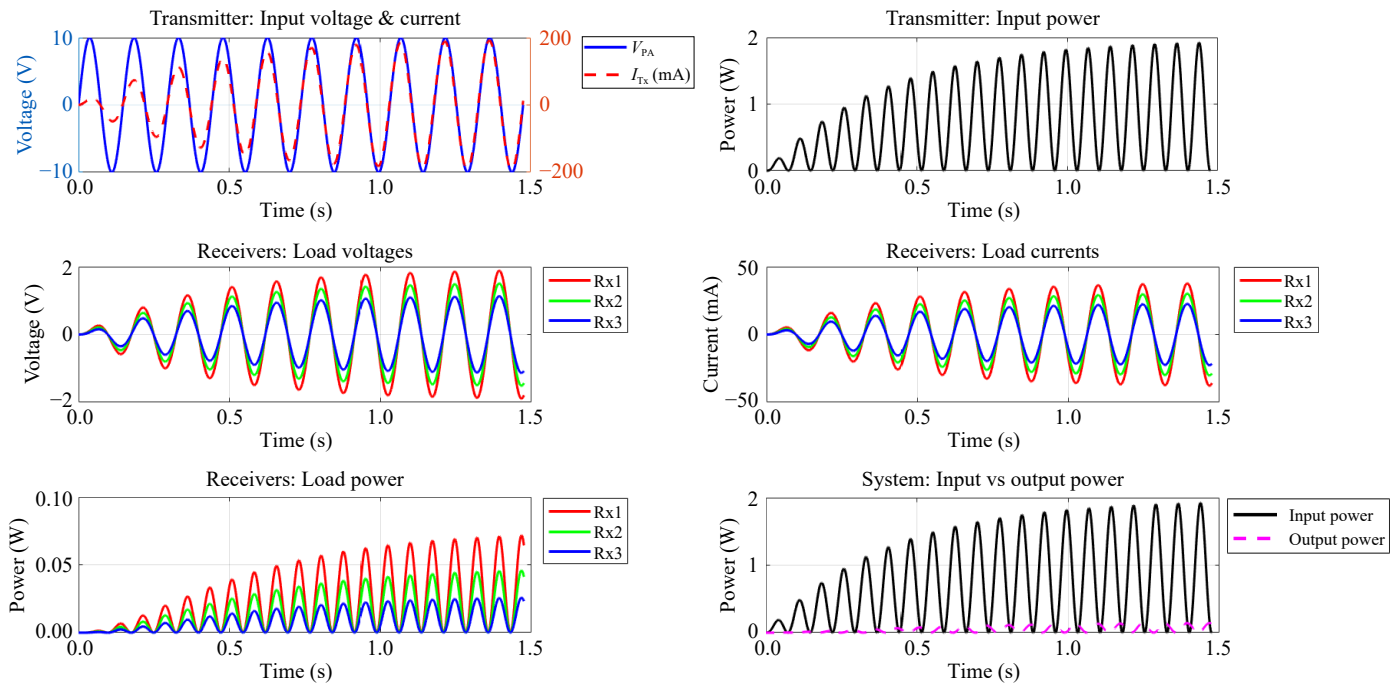

Fig. 11 Waveform diagram to illustrate the relationship between electrical parameters.

between −10 and 10 V, and current ranging from −200 to 200 mA. The second graph highlights the transmitter's input power, which peaks periodically at 2 W, representing the energy supplied to the system during operation. The third graph focuses on the load voltages of three receivers, Rx1, Rx2, and Rx3, exhibiting consistent oscillations between −2 and 2 V, which indicates uniform load conditions and functionality. The fourth graph captures the load currents of the receivers, which fluctuate within a range of −50 to 50 mA, demonstrating effective energy exchange between the transmitter and receivers. Additionally, the fifth graph illustrates the load power delivered to the receivers, reaching a peak of approximately 0.1 W, thereby showcasing efficient power distribution

among the receivers in multi-receiver scenarios. Finally, the sixth graph compares the input and output power of the system, revealing that the input gradually increases up to 2 W, while the output power remains stable around 0.1 W, underscoring the system's efficiency and steady performance. Together, these graphs emphasize the robust design and operational success of the WPT system.

Conclusions

This study presents a free-positioning WPT system tailored for applications involving multiple receivers. A strong magnetic field distribution is achieved in freedom[3] spatial by controlling the current direction. The mutual inductance is derived for the HCS-Tx

and a moving Rx to verify its stability. Additionally, the equivalent circuit of the multi-receiver WPT system is theoretically analyzed to formulate the power transfer efficiency (PTE) equation. The experimental findings validate that the proposed system efficiently transmits power to both single and multiple receivers. The proposed Tx coil can deliver power with an overall coil-to coil efficiency of 76.74% with a single receiver, and 96.14% with a multiple-receivers WPT system. These findings emphasize the capability of the proposed system to enhance power transfer performance and optimize energy distribution across multiple receivers. In addition, a wireless charging system was implemented to achieve 64% of the overall system efficiency. In conclusion, the WPT system using an HCS Tx coil presents a practical feasibility of a free-positioning wireless power transfer, catering to both single and multiple receivers with enhanced stability and performance.

To expand the scope of this research and enhance the practical applicability of the proposed wireless power transfer (WPT) system, several potential directions can be explored in future studies. One promising area is the investigation of system performance under varying power demands from multiple receivers, which would support stable and efficient operation in dynamic load conditions. Additionally, scaling the system to accommodate a larger number of receivers without degrading efficiency or increasing undesired cross-coupling remains an important challenge. This could be addressed through optimized coil designs or the development of advanced control and coordination strategies.

Future work could also focus on mitigating environmental factors such as temperature variations and electromagnetic interference while addressing practical concerns including hardware miniaturization and cost reduction. These efforts would contribute significantly to bridging the gap between experimental prototypes and real-world deployment, thereby advancing the realization of free-positioning WPT systems for diverse applications.

Author contributions

The authors confirm contribution to the paper as follows: study conception and design: Naveed I, Tan L; data collection: Naveed I, Hussain A; analysis and interpretation of results, draft manuscript preparation: Naveed I, Yameen MZ, Hussain A; funding acquisition and supervision: Tan L. All authors reviewed the results and approved the final version of the manuscript.

Data availability

All data generated or analyzed during this study are included in this published article.

Acknowledgments

Conflict of interest

The authors declare that they have no conflict of interest.

Dates

References

1. Song M, Belov P, Kapitanova P. 2017. Wireless power transfer inspired by the modern trends in electromagnetics. *Applied Physics Reviews* 4:021102

2. Zhao L, Thrimawithana DJ, Madawala UK, Hu AP, Mi CC. 2019. A misalignment-tolerant series-hybrid wireless EV charging system with integrated magnetics. *IEEE Transactions on Power Electronics* 34:1276−85

3. Kalra GR, Thrimawithana DJ, Riar BS, Huang CY, Neuburger M. 2020. A novel boost active bridge-based inductive power transfer system. *IEEE Transactions on Industrial Electronics* 67:1103−12

4. Campi T, Cruciani S, Maradei F, Feliziani M. 2019. Pacemaker lead coupling with an automotive wireless power transfer system. *IEEE Transactions on Electromagnetic Compatibility* 61:1935−43

5. Basar MR, Ahmad MY, Cho J, Ibrahim F. 2018. An improved wearable resonant wireless power transfer system for biomedical capsule endoscope. *IEEE Transactions on Industrial Electronics* 65:7772−81

6. Van Thuan N, Kang SH, Choi JH, Jung CW. 2015. Magnetic resonance wireless power transfer using three-coil system with single planar receiver for laptop applications. *IEEE Transactions on Consumer Electronics* 61:160−66

7. Zhang Y, Kan T, Yan Z, Mao Y, Wu Z, et al. 2019. Modeling and analysis of series-none compensation for wireless power transfer systems with a strong coupling. *IEEE Transactions on Power Electronics* 34:1209−15

8. Eteng AA, Rahim SKA, Leow CY, Jayaprakasam S, Chew BW. 2017. Low-power near-field magnetic wireless energy transfer links: a review of architectures and design approaches. *Renewable and Sustainable Energy Reviews* 77:486−505

9. Jonah O, Georgakopoulos SV, Tentzeris MM. 2013. Orientation insensitive power transfer by magnetic resonance for mobile devices. *2013 IEEE Wireless Power Transfer (WPT), 15−16 May, 2013, Perugia, Italy*. USA: IEEE. pp. 5−8 doi: 10.1109/WPT.2013.6556924

10. Hoang H, Lee S, Kim Y, Choi Y, Bien F. 2012. An adaptive technique to improve wireless power transfer for consumer electronics. *IEEE Transactions on Consumer Electronics* 58:327−32

11. Kim J, Kim DH, Park YJ. 2016. Free-positioning wireless power transfer to multiple devices using a planar transmitting coil and switchable impedance matching networks. *IEEE Transactions on Microwave Theory and Techniques* 64:3714−22

12. Kim J, Son HC, Kim DH, Park YJ. 2013. Impedance matching considering cross coupling for wireless power transfer to multiple receivers. *2013 IEEE Wireless Power Transfer (WPT), 15−16 May, 2013, Perugia, Italy*. USA: IEEE. pp. 226−29 doi: 10.1109/WPT.2013.6556924

13. Tan SY, Lee HJ, Lau KY, Ker PJ. 2018. Simulation of 4-coils magnetic resonance coupling for multiple receivers wireless power transfer at various transmission distance. *2018 IEEE Student Conference on Research and Development (SCOReD). 26−28 November, 2018, Selangor, Malaysia*. USA: IEEE. pp. 1−5 doi: 10.1109/SCORED.2018.8711181

14. Le-Huu H, Ha-Van N, Hong S, Seo C. 2019. Multiple-receiver wireless power transfer system using a cubic transmitter. *2019 IEEE Wireless Power Transfer Conference (WPTC). June 18−21, 2019. London, UK*. USA: IEEE. pp. 170−73 doi: 10.1109/wptc45513.2019.9055603

15. Kim YJ, Ha D, Chappell WJ, Irazoqui PP. 2016. Selective wireless power transfer for smart power distribution in a miniature-sized multiple-receiver system. *IEEE Transactions on Industrial Electronics* 63:1853−62

16. Kim J, Kim DH, Choi J, Kim KH, Park YJ. 2015. Free-positioning wireless charging system for small electronic devices using a bowl-shaped transmitting coil. *IEEE Transactions on Microwave Theory and Techniques* 63:791−800

17. Ha-Van N, Le-Huu H, Seo C. 2019. Design of free-positioning wireless power transfer using a half-rectangular prism transmitting coil. *2019 IEEE Wireless Power Transfer Conference (WPTC). 18−21 June, 2019. London, UK*. USA: IEEE. pp. 85−88 doi: 10.1109/wptc45513.2019.9055637

18. Ha-Van N, Seo C. 2018. Analytical and experimental investigations of omnidirectional wireless power transfer using a cubic transmitter. *IEEE Transactions on Industrial Electronics* 65(2):1358−66

19. Feng J, Li Q, Lee FC, Fu M. 2019. Transmitter coils design for free-positioning omnidirectional wireless power transfer system. *IEEE Transactions on Industrial Informatics* 15:4656−64

20. Liang Z, Wang J, Zhang Y, Jiang J, Yan Z, et al. 2019. A compact spatial

free-positioning wireless charging system for consumer electronics using a three-dimensional transmitting coil. *Energies* 12:1409

21. Beh TC, Kato M, Imura T, Oh S, Hori Y. 2013. Automated impedance matching system for robust wireless power transfer via magnetic resonance coupling. *IEEE Transactions on Industrial Electronics* 60:3689−98

22. Bito J, Jeong S, Tentzeris MM. 2016. A real-time electrically controlled active matching circuit utilizing genetic algorithms for wireless power transfer to biomedical implants. *IEEE Transactions on Microwave Theory and Techniques* 64:365−74

23. Li Y, Dong W, Yang Q, Zhao J, Liu L, et al. 2019. An automatic impedance matching method based on the feedforward-backpropagation neural network for a WPT system. *IEEE Transactions on Industrial Electronics* 66:3963−72

24. Jeong S, Lin TH, Tentzeris MM. 2019. Range-adaptive impedance matching of wireless power transfer system using a machine learning strategy based on neural networks. *2019 IEEE MTT-S International Microwave Symposium (IMS). 2−7 June, 2019, Boston, MA, USA*. USA: IEEE. pp. 1423−25 doi: 10.1109/mwsym.2019.8700996

25. Bertoluzzo M, Buja G, Dashora H. 2019. Avoiding null power point in DD coils. *2019 IEEE PELS Workshop on Emerging Technologies: Wireless Power Transfer (WoW). 18−21 June, 2019, London, UK*. USA: IEEE. pp. 11−15 doi: 10.1109/wow45936.2019.9030658

26. Manivannan B, Kathirvelu P, Balasubramanian R. 2023. A review on wireless charging methods – The prospects for future charging of EV. *Renewable Energy Focus* 46:68−87

27. Sample AP, Meyer DT, Smith JR. 2011. Analysis, experimental results, and range adaptation of magnetically coupled resonators for wireless power transfer. *IEEE Transactions on Industrial Electronics* 58:544−54

28. Zhang W, Zhang T, Guo Q, Shao L, Zhang N, et al. 2018. High-efficiency wireless power transfer system for 3D, unstationary free-positioning and multi-object charging. *IET Electric Power Applications* 12:658−65

29. Fu M, Yin H, Ma C. 2017. Megahertz multiple-receiver wireless power transfer systems with power flow management and maximum efficiency point tracking. *IEEE Transactions on Microwave Theory and Techniques* 65:4285−93

30. Riehl PS, Satyamoorthy A, Akram H, Yen YC, Yang JC, et al. 2015. Wireless power systems for mobile devices supporting inductive and resonant operating modes. *IEEE Transactions on Microwave Theory and Techniques* 63:780−90

31. Ahn D, Mercier PP. 2016. Wireless power transfer with concurrent 200-kHz and 6.78-MHz operation in a single-transmitter device. *IEEE Transactions on Power Electronics* 31:5018−29